Research Square

Preprints are preliminary reports that have not undergone peer review.
They should not be considered conclusive, used to inform clinical practice,
or referenced by the media as validated information.

Microbial community restructuring and shifts in carbohydrate-active enzyme coding potential along a decay gradient of standing dead moso bamboo culms

Yong Meng
State Key Laboratory of Woody Oil Resources Utilization
Meiqun Li
State Key Laboratory of Woody Oil Resources Utilization
Ming Yang
State Key Laboratory of Woody Oil Resources Utilization
Wensheng Ai
State Key Laboratory of Woody Oil Resources Utilization
Chao Peng
State Key Laboratory of Woody Oil Resources Utilization
Wende Yan
Faculty of Forestry, Central South University of Forestry and Technology
Minggao Chen
191731869710163.com

State Key Laboratory of Woody Oil Resources Utilization

Research Article

Keywords: standing dead culm, decay class, metagenomics, carbohydrate-active enzymes, auxiliary activities

Posted Date: November 16th, 2026

DOI: https://doi.org/10.21203/rs.3.rs-11461876/v1

License: This work is licensed under a Creative Commons Attribution 4.0 International License.
Read Full License

Additional Declarations: No competing interests reported.

Microbial community restructuring and shifts in carbohydrate-active enzyme coding potential along a decay gradient of standing dead moso bamboo culms

Yong Meng[a,b#], Meiqun Li[a,b#], Ming Yang[a], Wensheng Ai[a], Chao Peng[a], Wende Yan[b*], Minggao Chen[a*]

a State Key Laboratory of Woody Oil Resources Utilization, Hunan Academy of Forestry, Changsha, Hunan 410004, PR China

b Faculty of Forestry, Central South University of Forestry and Technology, 498 Shaoshan Southern Road, Tianxin District, Changsha City, Hunan 410004, PR China

*Corresponding author. E-mail: 19173186971@163.com

#These authors contributed equally to this work.

Abstract: Woody debris decomposition is central to carbon and nutrient cycling in terrestrial ecosystems, yet microbial community and functional gene dynamics in standing dead bamboo culms remain poorly understood. We sampled standing live and five decay classes (D1–D5) of dead moso bamboo culms in Hunan, China, and combined substrate chemistry with metagenomic analyses of taxonomic composition, carbohydrate-active enzyme (CAZy) coding potential, and bacterial metagenome-assembled genomes (MAGs). Across 18 composite samples, we assessed trends using stage-stratified bootstrap resampling. Along the D1–D5 gradient, cellulose and total carbon declined, while nitrogen and phosphorus concentrations increased. Microbial community composition shifted in an ordered manner across decay classes (PERMANOVA $R^2 = 0.303$, $P = 0.0001$), whereas fungal reads as a proportion of total reads decreased (Spearman $\rho = -0.753$). In the primary community-wide TPM analysis, auxiliary activities (AA) gene abundance ($\rho = -0.698$, $q = 0.0342$) and auxiliary redox function gene abundance ($\rho = -0.764$, $q = 0.0095$) declined with increasing decay class. Among AA genes with assignable taxonomic origins, fungal-assigned TPM decreased whereas bacterial-assigned TPM increased. Candidate bacterial MAGs provided genomic context for plant-polysaccharide utilization and auxiliary redox genes. These results demonstrate that standing dead moso bamboo decay is associated with shifts in substrate chemistry, community composition, and CAZy coding potential. The decline in auxiliary redox potential, accompanied by divergent fungal versus bacterial AA trends, suggests a functional transition between microbial domains during decay.

Keywords: standing dead culm; decay class; metagenomics; carbohydrate-active enzymes; auxiliary activities

1 Introduction

The decomposition of woody debris is a key component of carbon turnover and nutrient cycling in terrestrial ecosystems. Coarse woody debris (CWD) is both an important part of the forest carbon pool and a substrate for the long-term colonization of diverse fungi and bacteria. As decay progresses, the structural integrity and chemical composition of the wood are gradually altered, and components such as cellulose, hemicellulose, and lignin are utilized and transformed to varying degrees (Harmon et al., 1986; Cornwell et al., 2009; Weedon et al., 2009). The decomposition of woody debris is influenced by multiple factors, including tree species, the initial properties of the wood, temperature and moisture conditions, and the composition of the microbial community (van der Wal et al., 2015; Baldrian, 2017). During this process, structural carbon components are generally depleted over time, whereas the dry-weight concentrations of elements such as nitrogen and phosphorus may change owing to external inputs, microbial immobilization, or relative concentration following dry-matter loss. Changes in substrate conditions may alter microbial colonization and relative taxon abundance and may be accompanied by shifts in carbohydrate-active enzyme gene profiles and coding potential assigned to the auxiliary redox function. A joint assessment of substrate chemistry, microbial community composition, and CAZy coding potential is therefore needed to determine how these components covary during woody debris decay.

Moso bamboo (Phyllostachys edulis) is an important bamboo species in the subtropical regions of China and a major component of bamboo forest ecosystems. Previous studies have focused mainly on the decomposition of bamboo litter and on the effects of bamboo expansion and management practices on soil carbon fractions, nutrient cycling, and microbial communities (Shi et al., 2015; Dong et al., 2022; Huang et al., 2022), whereas the decay process of the dead culms themselves has received comparatively little attention.

After natural death, some moso bamboo culms remain upright as standing dead culms, creating a structural setting distinct from that of ground-level fallen logs. Standing dead culms have limited direct contact with the soil and are characterized by an upright, hollow structure that is continuously exposed to air; their moisture status, pathways of microbial immigration, and mode of substrate exposure may therefore differ from those of ground-level woody debris. These conditions may influence fungal and bacterial colonization and CAZy coding potential, yet integrated studies of substrate chemistry, microbial community composition, and coding potential in standing dead culms remain scarce. Standing dead bamboo therefore provides a distinct system for characterizing decay-class-associated variation in microbial communities and coding potential under upright conditions with limited soil contact.

Studies on tree deadwood and coarse woody debris indicate that wood decomposition is jointly influenced by host tree species, decay stage, and local environmental conditions. Fungal community composition varies with wood properties, host species, and decay class (Hoppe et al., 2016; Purahong et al., 2018; Mäkipää et al., 2017), and such variation can contribute to differences in wood decay rates (van der Wal et al., 2015; Perreault et al., 2023). Together, these findings suggest that community turnover across decay classes need not translate into a monotonic change in oxidative coding potential. Previous work has shown that fungal community assembly in standing deadwood shifts across decay stages (Chen et al., 2025), and that bacterial communities also respond to decomposition time, wood chemistry, and moisture conditions and may participate in the transformation of organic matter at different stages (Tláskal et al., 2017). Nevertheless, findings from fallen logs and standing deadwood of trees may not directly apply to standing dead bamboo because bamboo culms differ in structure and substrate organization. Existing research on bamboo, in turn, has focused largely on bamboo forest soils and litter processes. Overall, metagenomic studies that simultaneously analyze substrate chemistry, microbial community composition, and functional coding potential along a decay gradient in the bamboo culm itself remain limited.

Metagenomic sequencing can characterize standing dead culm decay at the levels of taxonomic composition and coding potential. Read-level classification characterizes the taxonomically assigned fraction of the community, whereas CAZy annotation estimates coding potential for plant-polysaccharide utilization, including genes in the auxiliary activities (AA) class and genes assigned to the auxiliary redox function (Yin et al., 2012; Lombard et al., 2014; Zhang et al., 2018; Zheng et al., 2023). Metagenome-assembled genomes (MAGs) can link a subset of these genes to candidate bacterial genomes(Bowers et al., 2017). Estimated gene-family abundance can be affected by sequencing depth, gene length, read mapping, assembly efficiency, and MAG recovery. We therefore used community-wide TPM as the primary metric and treated assembly- and MAG-based summaries as sensitivity analyses of trend direction.

We used a standing live culm reference group and five standing dead culm decay classes (D1–D5) from a moso bamboo forest in Taojiang, Hunan Province, and combined culm substrate chemistry with metagenomic analyses to address three questions. First, do the physically defined decay classes D1–D5 correspond to an ordered multivariate gradient in substrate chemistry? Second, does taxonomically resolved community composition shift in an ordered manner across decay classes, and does the relative contribution of fungal reads change along the same gradient? Third, does community-wide CAZy coding potential, particularly that of AA genes and the auxiliary redox function, show a consistent trend across decay classes after accounting for

sequencing depth and gene length, and which candidate bacterial MAGs provide partial genome-level context for the relevant CAZy genes? The primary community-wide analysis showed that coding potential assigned to the auxiliary redox function declined with increasing decay class, accompanied by decreasing fungal-assigned AA TPM and increasing bacterial-assigned AA TPM among genes with assignable taxonomic origins. The decreasing direction was retained under a stricter CAZy annotation threshold, although unnormalized summaries yielded a different trend.

2 Materials and Methods

2.1 Study area and sample collection

The study area is located in the Taohuajiang State-owned Forest Farm, Taojiang County, Yiyang City, Hunan Province, spanning 112°04′16″–112°06′59″ E and 28°18′25″–28°20′13″ N. The area lies in the hilly region of central Hunan, has a subtropical monsoon climate, and is dominated by yellow-brown earth soils.

This study focused on Moso bamboo (Phyllostachys edulis). In November 2025, samples were collected from old-aged standing live culms and from standing dead culms that had remained upright after natural death. Old-aged standing live bamboo was defined as bamboo with an age unit that remained physiologically viable, and served as the non-decayed control group (SLC); standing dead bamboo was divided into five decay classes, D1–D5, according to the degree of decay. The SLC group was used for comparison with standing dead bamboo of different decay classes but, because it does not belong to the decay sequence of standing dead bamboo, was not included in the ordered trend analysis of D1–D5.

A total of six sample groups were established, comprising one standing live culm control group and five decay-class groups of standing dead bamboo. Each group had three biological replicates, giving 18 composite samples in total. Each biological replicate corresponded to a 20 m × 20 m sampling area; the distance between the sampling areas of different replicates was no less than 20 m, and the distance between different culms within the same sampling area was no less than 2 m. Samples SLC_1–SLC_3 were the standing live culm controls; SDC1_1–SDC1_3, SDC2_1–SDC2_3, SDC3_1–SDC3_3, SDC4_1–SDC4_3 and SDC5_1–SDC5_3 corresponded to decay classes D1–D5, respectively. All samples, including D4 and D5, were collected from culms that remained in a standing (upright) position.

For each biological replicate of every decay class of standing dead bamboo, three mutually independent standing dead culms were collected. For samples with intact culm structure, subsamples were taken at the 1/4, 1/2, and 3/4 positions along the full length of the culm; for samples with a higher degree of decay and poorer culm integrity, subsamples were taken from the upper, middle, and lower parts of the collected culms. All sampling avoided the culm nodes.

Subsamples from the three positions of the same culm were first combined in equal amounts, and the samples from the three culms within the same sampling area were then combined in equal amounts to form one biological replicate sample. Immediately after collection, the samples were flash-frozen in liquid nitrogen and transported to the laboratory on dry ice, after which they were stored at −20 °C until DNA extraction and physicochemical analysis.

2.2 Decay-class classification and determination of substrate physicochemical properties

The decay classes of standing dead bamboo were defined with reference to established decay-classification schemes for coarse woody debris, adjusted to account for the structural characteristics of Moso bamboo culms. The classification indicators included culm color, structural integrity, material hardness, surface decay features, and the depth of knife penetration. Based on these indicators, the standing dead bamboo was divided into five classes, D1–D5: D1 represents the lowest degree of decay, with a relatively intact culm structure and hard material; D5 represents the highest degree of decay, with markedly disrupted culm structure and loose, friable material; and D2–D4 represent the continuous transitional stages between the two. The specific criteria for each decay class are provided in Table S1.

Cellulose, hemicellulose, lignin, total nitrogen, total phosphorus, total potassium, and total carbon contents were determined for the 18 culm samples. The samples were dried, ground, and homogenized as required by each assay. Cellulose, hemicellulose, and lignin were determined using a cellulose assay kit (JC0415-M), a hemicellulose assay kit (JC0416-M), and a lignin assay kit (JC2203-M; all kits from Nanjing Jice Biotechnology Co., Ltd., Nanjing, China), respectively.

For cellulose determination, cell-wall material was first extracted from the sample and starch was removed, after which cellulose was extracted using concentrated sulfuric acid. Following acid hydrolysis of cellulose to glucose, the anthrone colorimetric method was applied, absorbance was measured at 620 nm, and the cellulose content was calculated from a glucose standard curve. After hemicellulose had been converted to reducing sugars by acid treatment, the 3,5-dinitrosalicylic acid colorimetric method was applied, absorbance was measured at 540 nm, and the hemicellulose content was calculated from a xylose standard curve. After acetylation, lignin absorbance was measured at 280 nm, and the lignin content was calculated from the extinction coefficient of lignin. All of the above absorbance measurements were made using an Infinite 200 Pro M Nano microplate reader (Tecan, Switzerland), and the cellulose, hemicellulose, and lignin contents were all expressed on a sample dry-weight basis.

Total nitrogen content was determined by sulfuric acid digestion followed by the Kjeldahl method, in accordance with the Chinese agricultural standard NY/T 2419—2013. Approximately 0.2 g of homogenized sample was weighed, and a potassium sulfate–copper sulfate mixed catalyst

and concentrated sulfuric acid were added for digestion. After the sample had been digested to a clear solution, distillation and titration were carried out using a K1100 automatic Kjeldahl analyzer (Hanon, Jinan, China), and the total nitrogen content was calculated.

Total phosphorus and total potassium were determined by nitric acid–hydrogen peroxide microwave digestion combined with inductively coupled plasma mass spectrometry (ICP-MS). Approximately 0.1 g of dried sample was weighed, 5 mL of nitric acid and 1 mL of hydrogen peroxide were added, and the mixture was subjected to microwave digestion and acid removal before being made up to 50 mL. After filtration through a 0.22 μm membrane, the total phosphorus and total potassium contents of the solution were measured using a NexION 1000G inductively coupled plasma mass spectrometer (PerkinElmer, USA), with results expressed on a sample dry-weight basis.

Total carbon content was determined using a Vario EL III elemental analyzer (Elementar, Germany). Between 2 and 5 mg of dried, ground sample was weighed into a tin capsule and combusted at 1150 °C. The combustion products were detected after reduction and separation, and the results were corrected against reference materials. Total carbon content was expressed as a mass percentage on a sample dry-weight basis.

2.3 DNA extraction, library construction, and metagenomic sequencing

Immediately after collection, the samples were flash-frozen in liquid nitrogen, transported to the laboratory on dry ice, and stored at low temperature until DNA extraction. DNA purity was assessed using a NanoDrop spectrophotometer, DNA concentration was measured using a Qubit fluorometer, and DNA integrity was checked by 1% agarose gel electrophoresis. DNA that passed quality control was fragmented to approximately 300 bp using a Covaris M220 focused-ultrasonicator, after which paired-end sequencing libraries were constructed with the TruSeq DNA Sample Prep Kit. After the libraries had passed quality inspection, PE150 sequencing was performed on the Illumina NovaSeq platform. DNA extraction, library construction, and metagenomic sequencing were carried out by Genesky Biotechnologies Inc. (Nanjing, China)). Paired-end metagenomic sequencing data were obtained for all 18 samples. Each sample yielded 18.50–22.87 million raw reads, corresponding to 5.55–6.86 Gb of data; Q30 values ranged from 95.97% to 96.93% and GC content from 53.09% to 60.18%, indicating that the raw sequencing data were of overall good quality for all samples.

2.4 Quality control, host removal, and community classification

Raw paired-end reads were quality-controlled using fastp, including the removal of adapter sequences, low-quality bases, and reads that did not meet the length requirements. To reduce the influence of Moso bamboo host DNA on the microbial analysis, the Moso bamboo reference

genome GCA_036346405.1_KIB_Pedu_3 (*Phyllostachys edulis*) was used as the host reference sequence, and an index was built using Bowtie2. The quality-controlled paired-end reads were aligned to the Moso bamboo reference genome using the --very-sensitive mode of Bowtie2, after which SAMtools was used to retain read pairs in which neither end aligned to the host genome. The host-removed paired-end reads were used for the subsequent community classification, metagenomic assembly, MAG recovery, and functional analysis.

The average read-retention rate across the 18 samples was 99.61%, and the average Q30 of the quality-controlled reads was 98.41%. A total of 376,464,474 read pairs were obtained after quality control, of which 376,042,087 read pairs were retained after host removal. The read pairs removed because at least one end aligned to the Moso bamboo reference genome accounted for approximately 0.11%, indicating a low proportion of host sequences in the samples.

2.5 Community diversity and environmental association analyses

After removing human-related taxa, community diversity analyses were performed on the species-level abundance matrix generated by Bracken. Observed richness (number of observed taxa), the Shannon index, the Simpson index, and Pielou's evenness were calculated to describe the alpha diversity of each sample. Bray–Curtis distances were computed from the species-level relative abundances, and principal coordinates analysis (PCoA) was used to visualize differences in community composition among samples.

Differences in community structure among groups were assessed by permutational multivariate analysis of variance (PERMANOVA) using the adonis2 function of the vegan package (version 2.7-5) in R, with 9,999 permutations and the random seed set to 20260622. Three tests were conducted: the overall difference among all six sample groups, the overall difference among the five standing-dead-bamboo decay classes (D1–D5), and the linear trend when D1–D5 was treated as a numeric ordinal variable. The betadisper function was used to calculate the distance of each sample to its group centroid, and permutation tests were used to evaluate differences in multivariate dispersion among groups, in order to assess whether the PERMANOVA results might be influenced by unequal within-group dispersion.

To analyze the relationship between substrate physicochemical properties and microbial community composition, distance-based redundancy analysis (db-RDA) based on Bray–Curtis distances was performed on the 15 standing-dead-bamboo samples of D1–D5, with the standing live culm control excluded from this analysis. The db-RDA model was constructed using the capscale function, and the Bray–Curtis distances were additively corrected by setting add = TRUE.

The candidate explanatory variables were total nitrogen, total phosphorus, cellulose, total carbon, and lignin. Forward selection was performed using the ordiR2step function, with the adjusted coefficient of determination and permutation-test results used as the dual stopping criteria. The final model retained total nitrogen as the explanatory variable. The overall model significance, the significance of the constrained axis, and the effects of the explanatory variable were all evaluated with 9,999 permutations, with the random seed set to 20260622. Because total nitrogen was strongly correlated with total phosphorus, cellulose, total carbon, and lignin, the db-RDA result was used to characterize the statistical association between community composition and the coupled physicochemical gradient, and not to infer any independent causal effect of total nitrogen.

2.6 Metagenomic assembly, gene prediction, and CAZy annotation

The host-removed paired-end reads were assembled per sample using MEGAHIT (v1.2.9) with default parameters. After assembly, open reading frames were predicted from the assembled sequences of each sample using the metagenomic mode of Prodigal (v2.6.3; -p meta), yielding predicted genes and their encoded protein sequences.

The predicted protein sequences were aligned to a locally built CAZy protein database using DIAMOND blastp. The main parameters were set to --max-target-seqs 1 and --evalue 1e-5, retaining the best-matching hit for each query sequence. Based on the annotation of the best-matching protein, the predicted genes were assigned to the corresponding CAZy families and further aggregated into six functional classes: glycoside hydrolases (GH), glycosyltransferases (GT), carbohydrate esterases (CE), carbohydrate-binding modules (CBM), auxiliary activities (AA), and polysaccharide lyases (PL).

Based on a predefined mapping between CAZy families and substrate functions, the relevant CAZy families were further grouped into functions related to cellulose, hemicellulose/xylan, pectin, starch/oligosaccharides, and lignin-related auxiliary redox activity.

This analysis yielded the number of hits or genes of CAZy-annotated genes in the assembled sequences of each sample, without correction for sequencing depth, gene length, or read-mapping abundance. Therefore, these results were used only to describe the CAZy coding potential contained in the assemblies of different samples and were not treated as normalized CAZy gene abundances.

2.7 MAG recovery, classification, abundance estimation, and functional analysis

To obtain microbial taxonomic and functional information at the genome level, the host-removed paired-end reads of each sample were first re-aligned to the assembled sequences of the corresponding sample. Alignment was performed using the --very-sensitive mode of Bowtie2

(v2.5.1), and the resulting alignment files were sorted and indexed using SAMtools (v1.17). The coverage depth of each assembled sequence was then calculated using jgi_summarize_bam_contig_depths, and genome binning was performed per sample using MetaBAT2 (v2.15), with the minimum contig length for binning set to 1,500 bp.

The completeness and contamination of the candidate genome bins were evaluated using CheckM2 (v1.0.1). Bins with a length of at least 500 kb, completeness of at least 50%, and contamination below 10% were retained as medium-quality-or-higher candidate MAGs for subsequent analysis; among these, MAGs with completeness of at least 90% and contamination below 5% were flagged as candidate MAGs meeting the CheckM2 high-quality threshold. Because rRNA, tRNA, and other MIMAG criteria were not comprehensively assessed, these are not referred to here as high-quality MAGs in the strict sense.

The medium-quality-or-higher candidate MAGs were dereplicated using dRep (v3.4.5), with the average nucleotide identity (ANI) threshold set to 95% for the main analysis and the dereplication result at a 99% threshold used as a sensitivity analysis. Taxonomic annotation of the dereplicated representative MAGs was performed using GTDB-Tk (v2.4.0) with the GTDB release 232 database, running the identify, align, and classify workflows in sequence. Because this MAG recovery and quality-evaluation pipeline was designed primarily for prokaryotes, the MAG-level taxonomic and functional results represent only the bacterial genome fraction recoverable in this study.

The abundance of each representative MAG in each sample was estimated using CoverM genome (v0.7.0). The host-removed reads of the 18 samples were competitively mapped to the dereplicated set of representative MAGs, with the minimum sequence identity set to 95% and the minimum aligned-length fraction set to 75%, outputting relative abundance, mean coverage, and covered fraction. Reads that did not map to the representative MAG set were counted separately and were not included in the calculation of relative abundance within the MAG set. Therefore, the MAG relative abundances reported here represent the relative abundance of each MAG within the recovered set of representative MAGs, and are not interpreted as their absolute proportion in the entire microbial community.

Protein-coding genes in the representative MAGs were predicted using Prodigal (v2.6.3). The predicted proteins were searched against the dbCAN HMM database using HMMER (v3.4) and against the CAZy protein database using DIAMOND blastp; the database versions were dbCAN v5.2 and CAZyDB 07242025, respectively. DIAMOND alignment used the best-matching hit with an E-value threshold of 1×10^{-5}. An annotation was accepted as a high-

confidence CAZy annotation only when HMMER and DIAMOND assigned the same protein to the same CAZy family.

The high-confidence CAZy annotations were aggregated into the six functional classes (GH, GT, CE, CBM, AA, and PL) and, based on the predefined mapping between CAZy families and functional roles, further grouped into functions related to cellulose, hemicellulose/xylan, pectin, starch/oligosaccharides, and lignin-related auxiliary redox activity.

The selection of candidate functional-carrier MAGs jointly considered genome completeness and contamination, taxonomic annotation, sample abundance, decay-stage preference, and the presence of high-confidence CAZy functional roles. A MAG was defined as a stage-preferential candidate MAG for a given decay class when its group-mean relative abundance in that class was $\geq 0.5\%$ and at least twice the group mean of the second-highest decay class. This selection is a descriptive analysis; it did not employ a replicate-based differential-abundance model and did not apply the corresponding correction for multiple testing. Accordingly, these MAGs are consistently described as "stage-preferential candidate MAGs" or "candidate functional carriers" rather than as "significantly enriched MAGs" or "validated key degraders."

2.8 Construction of the non-redundant gene catalogue and statistical analysis

To reduce the influence of differences in sequencing depth and MAG recovery among samples on the functional comparison, the predicted gene sequences from the assemblies of all 18 samples were combined, and a non-redundant gene catalogue was constructed using MMseqs2. The sequence-clustering thresholds were set to 95% nucleotide identity and 90% coverage. One representative sequence was selected for each gene cluster and used for the subsequent read mapping and functional-abundance calculation.

The host-removed paired-end reads of each sample were competitively mapped to the non-redundant gene catalogue. Mapping was performed with CoverM contig calling minimap2-sr, with the minimum sequence identity set to 95% and the minimum aligned-length fraction set to 75%. Based on the mapping results, the read count and TPM of each representative gene in each sample were calculated. TPM, which corrects simultaneously for gene length and sample sequencing depth, was used as the primary metric for community-wide comparison of CAZy functional abundance.

The original CAZy annotations of each sample were projected onto the representative genes according to the membership of the MMseqs2 gene clusters, and the CAZy family of each representative gene was determined by a family-majority-consensus approach. When a given CAZy family accounted for no less than 0.80 of the valid annotations within the same gene cluster, that family was assigned to the corresponding representative gene; gene clusters that did

not reach this threshold were flagged as low-consensus and were excluded from the main CAZy abundance analysis. For the representative genes with high-consensus annotations, TPM was aggregated at three levels: CAZy family, functional class, and substrate functional role.

To test whether the results were affected by the normalization method, four approaches were compared for sensitivity: normalization to the number of predicted ORFs from the assemblies, mapping to CAZy reference sequences, MAG-abundance-weighted analysis, and non-redundant gene catalogue TPM analysis. Among these, ORF-number normalization corrects only for the total number of predicted ORFs per sample and does not correct for gene length or read-mapping abundance; it therefore served only as a sensitivity analysis and did not replace the TPM results calculated from the non-redundant gene catalogue.

The potential taxonomic origin of the CAZy representative genes was determined by combining the Tiara classification of the contig on which each gene was located with the OX= taxonomic identifier in the Swiss-Prot annotation, in order to estimate the bacterial and fungal origins of the assignable CAZy genes. Representative genes for which Tiara and Swiss-Prot (OX classification) disagreed at the domain level were uniformly assigned to "origin undetermined" and were excluded from the fungal/bacterial source partitioning. Representative genes whose taxonomic origin could not be reliably determined were classified as origin undetermined. Because the taxonomic origin of some CAZy representative genes could not be resolved, this analysis reflects only the source composition of the assignable CAZy genes or TPM, and does not represent the absolute source proportions of all sequenced reads or of all CAZy genes.

Unless otherwise stated, all statistical analyses used the composite samples as the basic analytical unit, that is, three biological replicates per group. SLC served as the standing live culm control for among-group comparisons, whereas the 15 standing-dead-bamboo samples of D1–D5 were used for the ordered decay-trend analysis. D1–D5 were coded as 1–5, and Spearman's rank correlation was used to test the monotonic relationship between continuous variables and decay class.

To assess the stability of the trend results, the three biological replicates within each decay class were resampled with replacement, and 10,000 stratified bootstrap iterations were performed, with 95% confidence intervals calculated by the percentile method. The random seed was set to 20260622. For multiple comparisons within the same analysis series, P values were corrected for the false discovery rate using the Benjamini–Hochberg method, and the corrected q values are reported. Unless otherwise stated, two-sided $P < 0.05$ or $q < 0.05$ was used as the criterion for statistical significance.

All statistical analyses and graphical work were carried out in R and Python. All CAZy annotation, MAG function, and gene catalogue results are interpreted as genomic coding potential and do not represent gene transcription, protein abundance, enzyme activity, or actual metabolic flux.

Funding

This work was supported by the 2025 Provincial Bamboo Industry Development Project (No. 2025ZCY003) and the Hunan Provincial Forestry Science and Technology Innovation Program (No. XLK202505).

3 Results

3.1 Substrate chemical properties vary systematically but in contrasting directions across decay classes

Along the D1–D5 decay gradient, different chemical indicators of the culm substrate changed in contrasting directions (Fig. 1; Table S1; n = 3 per decay class, 15 samples in total). The group-mean dry-mass concentration of total nitrogen increased from 2.64 mg g^{-1} at D1 to 14.15 mg g^{-1} at D5 and was strongly positively correlated with decay class (Spearman $\rho = 0.960$; stratified bootstrap 95% CI: 0.920–0.992; $q < 0.001$). Total phosphorus content likewise increased with advancing decay ($\rho = 0.949$; 95% CI: 0.892–0.991; $q < 0.001$). In contrast, both cellulose and total carbon contents declined as the decay class increased, with correlation coefficients of −0.786 (95% CI: −0.954 to −0.646; $q < 0.001$) and −0.633 (95% CI: −0.845 to −0.427; $q = 0.013$), respectively.

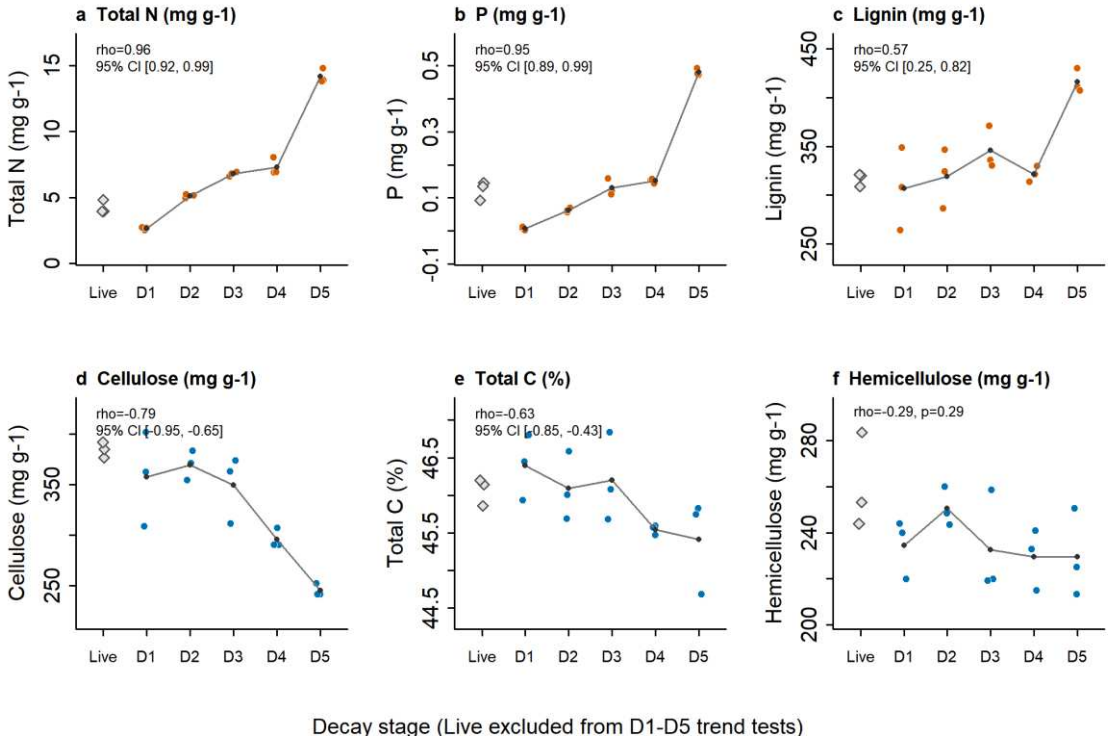


Fig. 1 Decay classes of standing dead bamboo correspond to ordered changes in substrate chemistry. Six substrate indicators across the standing live culm reference (SLC) and decay classes D1–D5. Points are biological replicates; grey lines connect D1–D5 group means. Spearman's ρ with stage-stratified bootstrap 95% CIs (D1–D5 only) are shown in each panel. All measurements are expressed on a dry-mass basis; the units for individual variables are shown on the corresponding y-axes.

Lignin content increased overall with decay class and reached its maximum at D5, although the change was not strictly monotonic between adjacent classes (ρ = 0.567; 95% CI: 0.252–0.824; q = 0.029). Hemicellulose content fluctuated among decay classes without a clear ordered trend. Overall, the decay of standing dead bamboo was characterized by declining cellulose and total carbon contents alongside rising total nitrogen and total phosphorus contents.

Because these variables were expressed on a dry-mass basis, the increases in total nitrogen, total phosphorus, and lignin describe changes in concentration and do not establish increases in their absolute stocks. The standing live culm samples served as a living reference and were excluded from D1–D5 trend analyses because they were not part of the standing dead culm decay sequence, and were therefore excluded from the correlation analyses along the D1–D5 gradient.

3.2 Microbial community composition varies across decay classes and covaries with substrate chemistry

Among the D1–D5 standing dead bamboo samples, the composition of the classifiable microbial community differed significantly among decay classes (Fig. 2a, b). PERMANOVA based on species-level Bray–Curtis distances showed that decay stage explained 56.8% of the compositional variation ($R^2 = 0.568$, $p = 0.0003$). When D1–D5 was modelled as an ordinal variable, decay class still explained 30.3% of the variation ($R^2 = 0.303$, $p = 0.0001$), supporting a linear compositional trend across the ordered D1–D5 decay classes. This ordered compositional shift is evident in the species-level PCoA (Fig. 2c). This shift was consistent across the species and genus levels and across three read-filtering schemes (ordered model $R^2 = 30.3\%–33.8\%$; $p \leq 0.0003$; Table S2), Multivariate dispersion did not differ detectably among decay classes across these analyses (betadisper, $P \geq 0.40$), providing no evidence that the PERMANOVA results were attributable to unequal within-group dispersion. Inclusion of the standing live culm reference group resulted in a stronger overall separation among the six groups; because these culms remained physiologically active and lie outside the decay sequence, subsequent trend analyses were restricted to D1–D5.

In contrast to this compositional shift, alpha diversity varied little across decay classes (Shannon 7.52–7.97; Simpson ≈ 0.998; no significant among-group differences, Table S2). The detectable community response was therefore expressed primarily as a change in relative taxonomic composition rather than as a directional change in alpha diversity. Among the dominant phyla, Pseudomonadota tended to be more abundant at later stages but was non-significant after multiple-testing correction ($\rho = 0.524$, $q = 0.158$). Ascomycota, which accounted for nearly all classifiable fungal reads, declined significantly with decay ($\rho = -0.753$, $q = 0.0084$; stratified bootstrap 95% CI: −0.954 to −0.462) (Fig. 2d); the decrease in fungal-read proportion and the decrease in Ascomycota therefore represent a single signal rather than two independent lines of evidence.

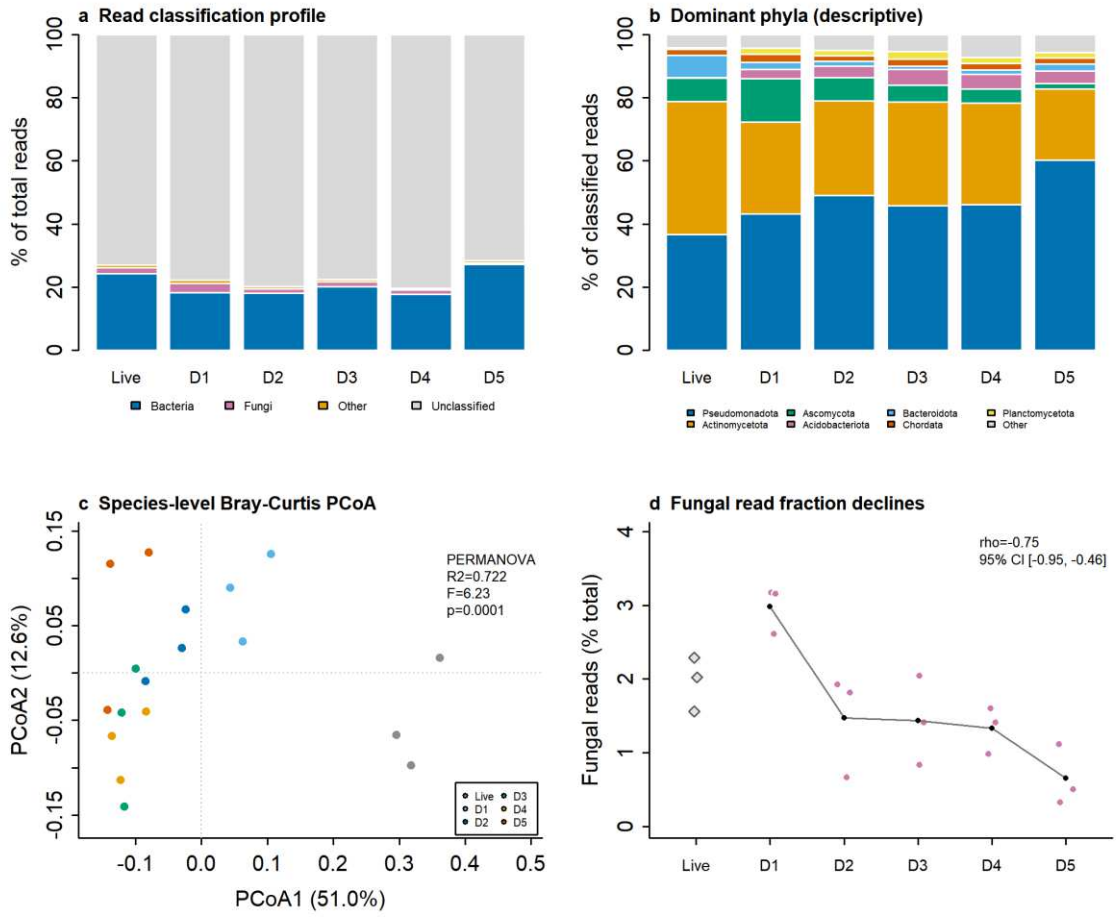


Fig. 2 Classifiable microbial community composition differs along the decay gradient. (a) Read-level taxonomic composition at each stage, as a percentage of total reads. (b) Group-mean composition of the dominant phyla within the classifiable community. (c) Species-level Bray–Curtis PCoA after removal of Homo sapiens; PERMANOVA used vegan::adonis2 with 9,999 permutations. (d) Proportion of fungal reads relative to total reads; trend analysis used D1–D5 only. Community-level conclusions refer to classifiable reads only.

3.3 The substrate-chemistry gradient is associated with microbial community composition

To examine the relationship between substrate chemistry and microbial community composition, db-RDA based on Bray–Curtis distances was performed on the 15 standing dead bamboo samples of D1–D5 (Fig. 3). Forward selection among total nitrogen, total phosphorus, cellulose, total carbon, and lignin retained total nitrogen as the only variable in the final model. The resulting one-variable model accounted for 26.6% of the compositional variation (adjusted R^2 = 0.210, pseudo F = 4.721, P = 0.0005; residual df = 13). Because decay class was not included as a conditioning variable, this model describes covariation along the D1–D5 gradient and does

not estimate an association with total nitrogen independent of decay class. (adjusted 21.0%; F = 4.721, P = 0.0005, residual df = 13). Total nitrogen was strongly correlated with total phosphorus (Spearman ρ = 0.882) and negatively correlated with cellulose and total carbon (ρ = −0.761 and −0.650; Fig. 3c). Given these correlations, total nitrogen was interpreted as a statistical proxy for the coupled nutrient–structural-carbon gradient rather than as a uniquely supported explanatory variable.

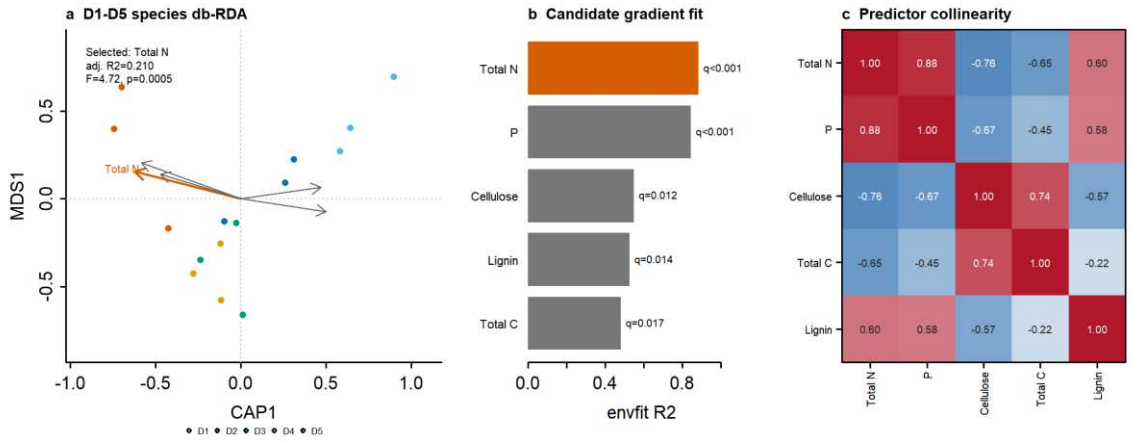


Fig. 3 Community restructuring is associated with a coupled substrate-chemistry gradient. (a) Species-level db-RDA for D1–D5. The species matrix excluded Homo sapiens and was pre-filtered to taxa detected in at least two samples with abundance ≥ 1 × 10^{-5} (as a proportion). The constrained db-RDA model included total nitrogen as its only explanatory variable. Arrows for all five chemical variables represent post hoc envfit projections and were not simultaneous constraints in the db-RDA model (b) envfit R^2 and BH-adjusted q for the candidate variables. (c) Spearman correlation matrix among the candidate variables. Total nitrogen is a statistical proxy for the coupled gradient and does not represent an independent causal driver.

3.4 Representative MAG recovery and total abundance differ markedly among stages

Metagenomic assembly, binning, quality assessment, and dereplication at 95% ANI yielded 117 representative bacterial MAGs (Fig. 4; Table S3), spanning 13 bacterial phyla and dominated by Pseudomonadota, Actinomycetota, Acidobacteriota, and Bacteroidota. The number of representative MAGs recovered per group varied markedly: D1 and D2 contributed 5 MAGs each, whereas D3, D4, D5, and the standing live culm control contributed 23, 18, 42, and 24, respectively—indicating substantially fewer MAGs recovered from D1 and D2 than from the other groups.

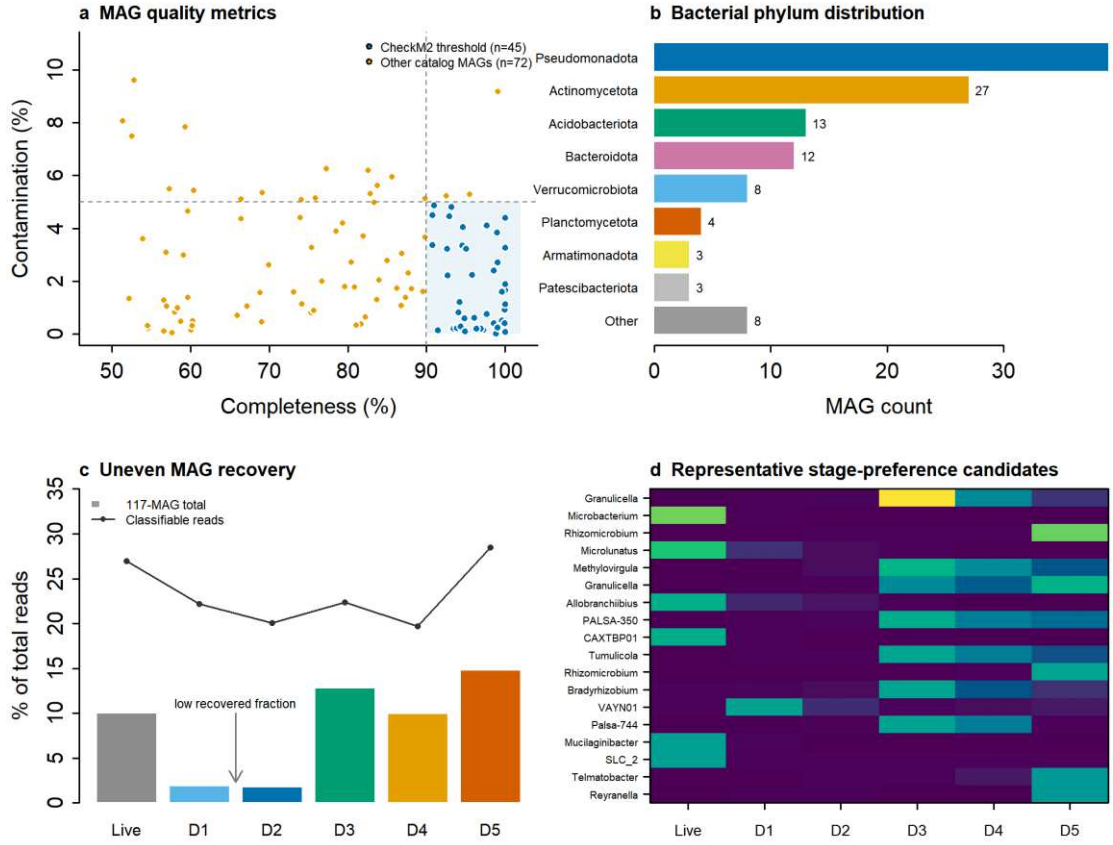


Fig. 4 The 117 bacterial MAGs form a genome dataset shaped by stage-dependent recovery bias. (a) MAG completeness versus contamination; shading marks the CheckM2 threshold region (completeness ≥ 90%, contamination ≤ 5%). (b) Phylum-level composition of the MAG count. (c) Total 117-MAG abundance per stage alongside the proportion of PlusPF-classifiable reads, showing markedly lower MAG recovery at D1–D2. (d) Heatmap of group-mean abundances for representative stage-preferential candidate MAGs, defined by group-mean and fold-change rules without a replicate-based differential-abundance test. Given the low MAG recovery at D1–D2, genus-level comparisons involving these two stages should be interpreted with caution.

The total relative abundance of the 117 representative MAGs showed a similar pattern, with group means for SLC and D1–D5 of 10.04%, 1.96%, 1.83%, 12.87%, 9.99%, and 14.87%, respectively; D1 and D2 were clearly lower than the other classes. Read-level taxonomy showed no comparable decline in microbial reads at D1 and D2, so the lower MAG recovery and total abundance at these stages most likely reflect the assembly characteristics, community complexity, or binning efficiency of these samples rather than a lower total microbial load.

The MAG recovery and quality-assessment pipeline used here targeted prokaryotes and did not employ eukaryote-specific assembly, binning, or genome-quality methods; consequently, no fungal genomes were obtained in the representative MAG set. This does not imply the absence of fungi, but means that the MAG-level taxonomic and functional analyses represent only the recoverable bacterial fraction and do not capture the full community detected at the read level, and in particular do not represent the fungal community.

3.5 In the community-wide normalized CAZy profile, AA coding potential declines with increasing decay

To limit the influence of uneven MAG recovery on the functional trends, community-wide CAZy gene abundances were recalculated from the unified non-redundant gene catalogue, using TPM to correct for gene length and sequencing depth (Fig. 5). Across D1–D5, the TPM of auxiliary activity (AA)-class CAZy genes declined with increasing decay class (Spearman $\rho = -0.698$, $q = 0.0342$), and the direction was unchanged under a stricter CAZy annotation threshold ($\rho = -0.676$, $q = 0.0402$). The AA share of total CAZy TPM also declined with decay ($\rho = -0.917$, $q = 0.0006$), as did auxiliary redox function ($\rho = -0.764$, $q = 0.0095$).

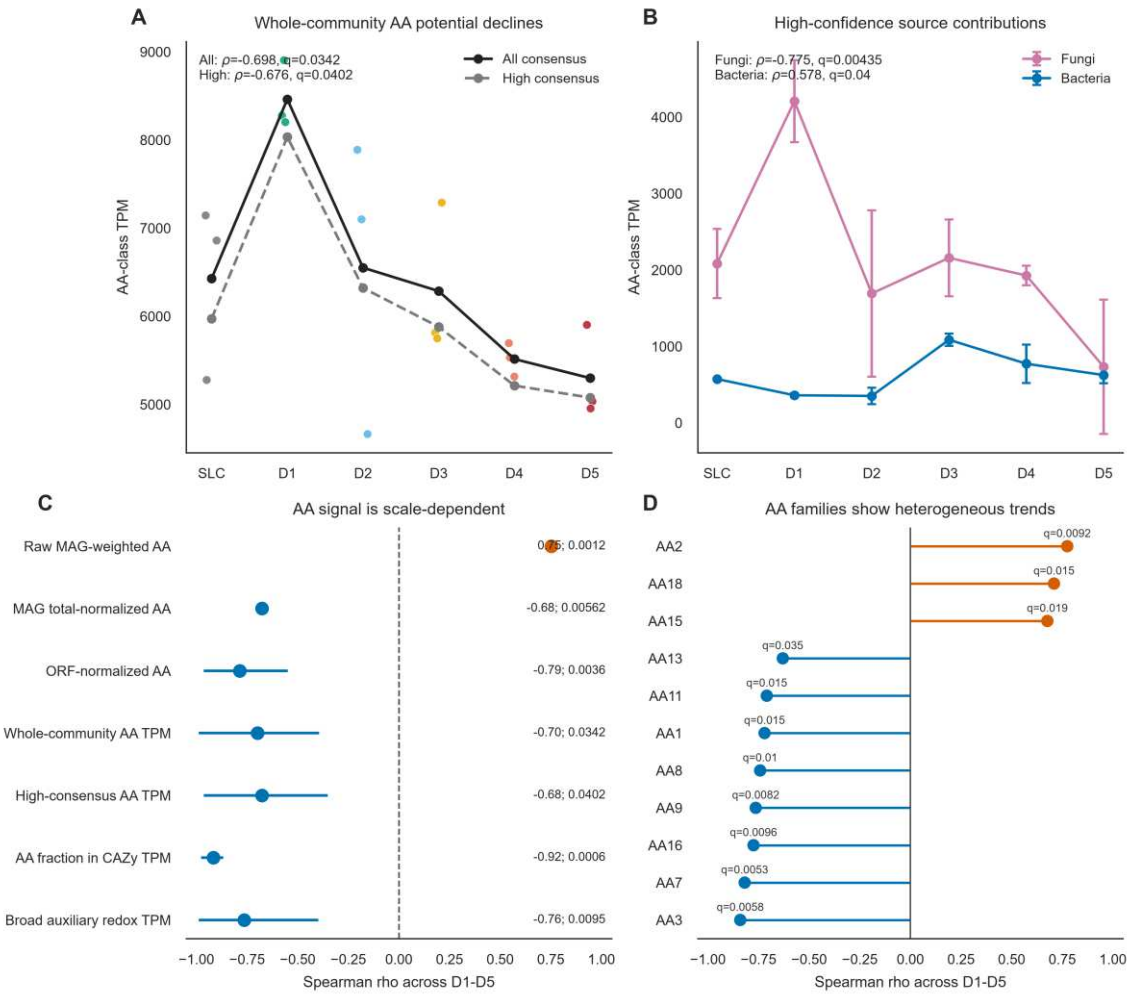


Fig. 5 Community-wide normalized CAZy analysis shows a decline in AA / auxiliary redox coding potential. (a) Change in AA-class CAZy TPM across D1–D5. (b) Decay-class trends in AA TPM assigned concordantly to fungi or bacteria. (c) Direction of AA trends under alternative normalization methods. Values from different methods have distinct denominators and are not directly comparable in magnitude. (d) Trends of AA families that changed significantly. Trend tests apply to D1–D5 only; SLC is shown as the standing live culm reference.

This direction was not uniform across normalization scales: unnormalized assembly gene counts indicated an increase in AA genes with decay, whereas normalization to total MAG abundance, to ORF number, and to community-wide TPM all indicated a decrease. Because unnormalized counts are sensitive to sequencing depth, assembly efficiency, predicted ORF number, and MAG recovery, we base the interpretation of AA coding potential on the normalized results.

Partitioning the AA genes of determinable origin showed that fungal-derived AA TPM declined with decay ($\rho = -0.775$, $q = 0.0044$), whereas bacterial-derived AA TPM increased ($\rho =$

0.578, q = 0.040). The community-wide decline in AA coding potential thus does not reflect a synchronous weakening of AA functions across all microbial sources, but rather a decrease in the fungal-derived AA signal alongside an increase in the bacterial-derived signal. Because this partitioning depends on the classification of CAZy representative genes and their contigs, and some genes could not be assigned, it reflects the source composition of the assignable AA genes only.

At the family level, most AA families that changed significantly declined with decay, but AA2, AA15, and AA18 increased, indicating divergent directions and a potential division of function within the AA class. These family-level results indicate restructuring of AA coding potential rather than a uniform decline across all AA families.

3.6 Candidate bacterial MAGs show descriptive decay-class preferences in abundance and CAZy composition

Fifteen candidate bacterial MAGs were selected from the 117 representatives using predefined criteria based on genome quality, taxonomic assignment, group-mean abundance, decay-class preference, and CAZy composition (Fig. 6; Table S4). on the basis of genome quality, taxonomic annotation, sample abundance, and CAZy functional composition (thresholds in Methods; Fig. 6; Table S4). Most candidate MAGs simultaneously carried CAZy families associated with cellulose, hemicellulose/xylan, pectin, and starch/oligosaccharide utilization, showing that individual candidate MAGs contained coding potential associated with multiple plant-polysaccharide functional categories.

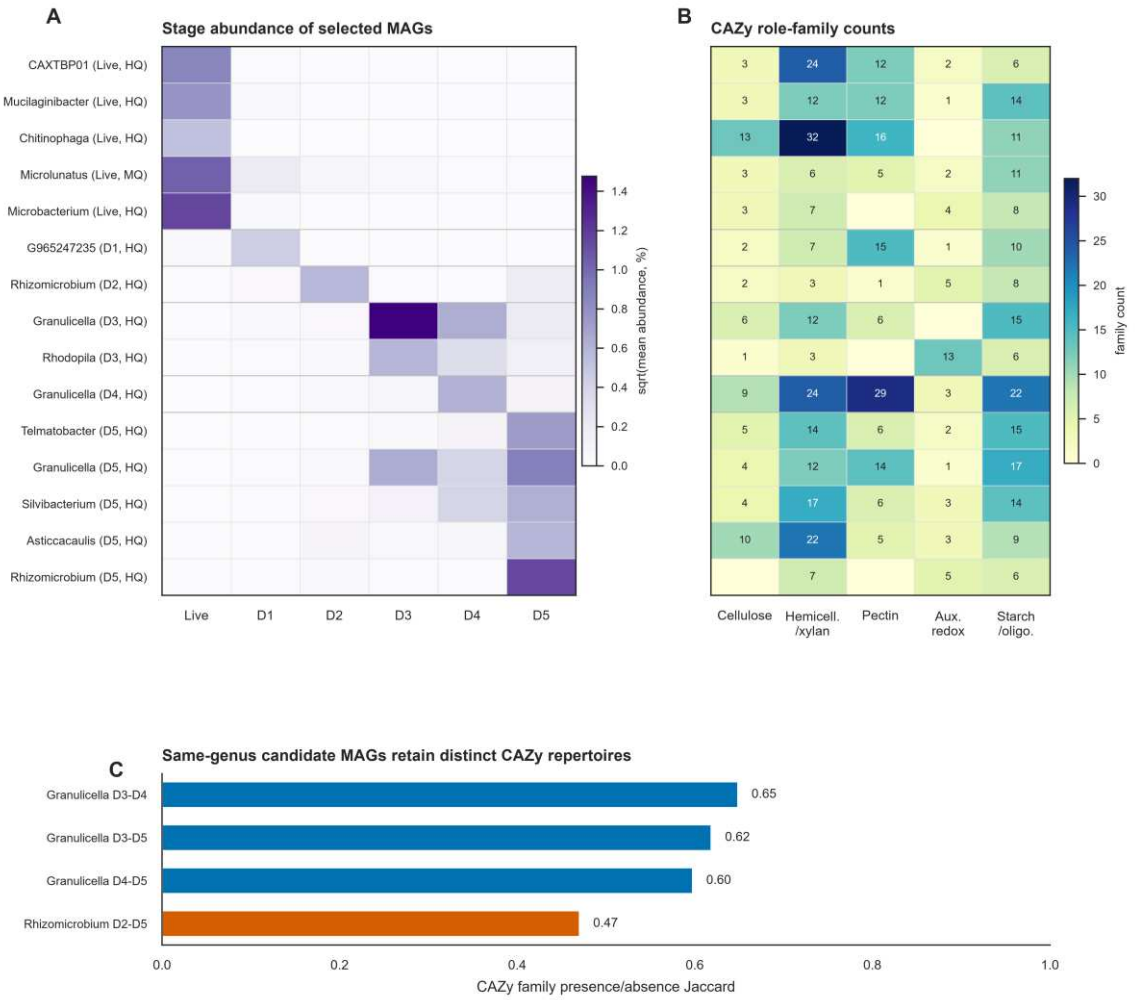


Fig. 6 Stage distribution and potential functional contribution of the candidate bacterial MAGs. (a) Mean relative abundance of the 15 candidate bacterial MAGs across the standing live culm reference and D1–D5. (b) Number of CAZy role families for plant-polysaccharide utilization and auxiliary redox function carried by each candidate MAG. (c) Presence/absence similarity of CAZy families among candidate MAGs of the same genus. The figure shows candidate functional carriers among the recoverable bacterial genomes and does not represent validated degraders or actual enzyme activity; given the low MAG recovery at D1–D2, candidate comparisons involving these stages should be interpreted with caution.

The composition of high-abundance candidate MAGs differed among decay stages. Several Granulicella MAGs abundant at D3, D4, and D5 carried numerous CAZy families related to hemicellulose/xylan, pectin, and oligosaccharide utilization. A Rhizomicrobium MAG preferential to D5 and a Rhodopila MAG preferential to D3 carried multiple auxiliary redox-related CAZy families. The CAXTBP01 and Microbacterium MAGs abundant in the standing live culm control showed CAZy family combinations distinct from these standing-dead-bamboo

candidates. These MAGs provide candidate bacterial genomic contexts for a subset of the CAZy genes detected in the community-wide analysis (Fig.7).

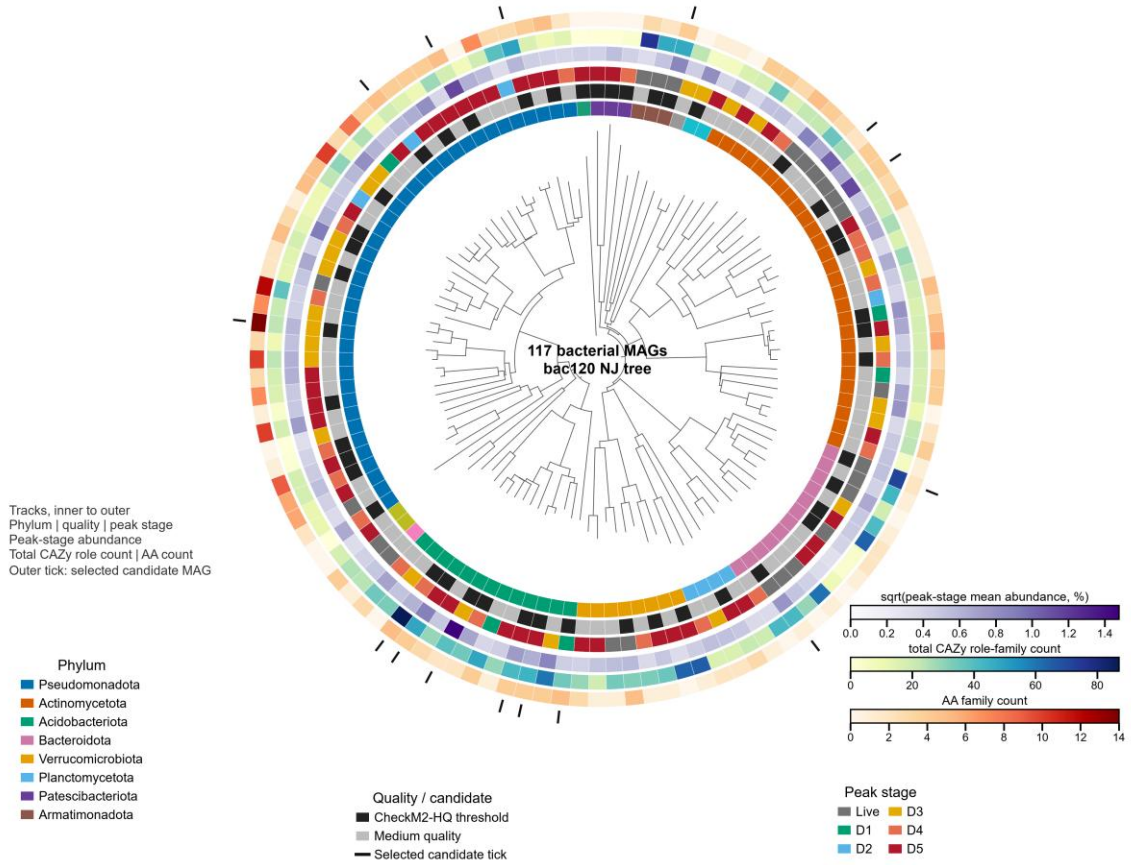


Fig. 7 Phylogenetic distribution, peak stage, and CAZy coding potential of the recoverable bacterial MAGs. The central tree comprises the 117 representative bacterial MAGs, inferred from bac120 marker genes. Concentric rings (inner to outer) show: phylum, MAG quality tier, the stage of each MAG's highest mean relative abundance (peak stage; SLC and D1–D5), square-root-transformed peak-stage abundance, total CAZy functional-role family count, AA-class family count, and candidate functional-carrier flags (outer black ticks). The figure represents only the recoverable bacterial fraction and excludes fungi and unbinned genomes.

Decay-class preference was defined descriptively from group means and fold-change thresholds without replicate-based differential-abundance testing. Accordingly, the selected MAGs are described as candidate bacterial functional carriers with CAZy coding potential

associated with plant-polysaccharide utilization, rather than as significantly enriched taxa or experimentally validated key degraders.

4 Discussion

Across the D1–D5 decay gradient, this study documented concurrent variation in substrate chemical properties, microbial community composition, and CAZy coding potential in standing dead culms. As decay advanced, culm cellulose and total carbon declined while dry-weight nitrogen and phosphorus concentrations rose; the classifiable community underwent an ordered restructuring in which the relative contribution of fungal sequences decreased; and community-wide normalized analysis showed an overall decline in AA and auxiliary redox coding potential, accompanied by divergent trends in fungal- and bacterial-assigned AA coding potential and heterogeneous responses among AA families. Candidate bacterial MAGs provided genomic contexts for a subset of the bacterial CAZy genes detected in the community-wide analysis. The principal functional result was that normalized AA-class and auxiliary redox-function coding potential decreased rather than increased monotonically across D1–D5. This pattern characterizes standing dead culms at the study site but does not establish a functional succession distinct from that of fallen logs, which were not sampled.

4.1 Decay classes correspond to a broadly ordered gradient in culm substrate chemistry

The correspondence between physical decay classes and substrate chemistry supports the use of D1–D5 as an ordered gradient of culm substrate state. However, the measured components did not change synchronously: cellulose and total carbon decreased, dry-mass nitrogen and phosphorus concentrations increased, and lignin and hemicellulose showed less uniform patterns. Thus, D1–D5 represent a multivariate gradient dominated by structural-carbon loss and increasing dry-mass nutrient concentrations. More broadly, wood traits contribute to interspecific variation in decomposition rates (Cornwell et al., 2009; Weedon et al., 2009), while deadwood density and carbon concentration can vary systematically among decay classes (Shorohova et al., 2022). Higher dry-mass nitrogen and phosphorus concentrations may reflect relative concentration as carbon-rich material is lost, but the absence of mass-balance measurements prevents separation of relative concentration from nutrient retention or microbial immobilization.

This physical–chemical correspondence provides a substrate-state framework for interpreting the accompanying community and functional variation. Moso bamboo culms contain vascular bundles embedded in ground parenchyma and exhibit pronounced radial variation in vascular-bundle morphology and distribution (Tsuyama et al., 2023). This anatomical

heterogeneity could contribute to spatial variation in substrate accessibility during decay, although the present study did not test tissue-specific decomposition.

Because each composite sample integrated multiple longitudinal positions but did not separate vascular bundles, parenchyma, or radial tissue layers, tissue-specific chemical changes could not be resolved.

4.2 Community composition covaries with substrate state, while the relative fungal signal declines

Community composition differed among the six groups, including the standing live culm reference, and showed a linear compositional trend across the D1–D5 standing dead culm samples. The absence of a statistically supported trend in the evaluated alpha-diversity metrics, despite clear Bray–Curtis differentiation, indicates that within-sample diversity can remain broadly stable while taxonomic relative abundances are redistributed among decay classes. The direction of this compositional trend was consistent across the evaluated taxonomic levels and read-filtering schemes, and no difference in multivariate dispersion was detected, supporting robustness to these specific analytical choices. Community differentiation among decay classes has also been reported for deadwood-associated fungi and bacteria (van der Wal et al., 2015; Hoppe et al., 2016; Tláskal et al., 2017), although the present cross-sectional design does not resolve temporal succession within individual culms.

Community composition covaried with a coupled gradient of decreasing cellulose and total carbon and increasing dry-mass nitrogen and phosphorus concentrations. Because these chemical variables were strongly correlated and decay class was not included as a conditioning variable, the retention of total nitrogen by forward selection does not identify nitrogen as a unique ecological driver. Instead, total nitrogen represents one statistical proxy for substrate changes that occurred concurrently with community restructuring.

The proportion of fungal reads decreased overall along the D1–D5 gradient, indicating a weakening of the relative fungal signal in the metagenomic data. Limited soil contact and differences in culm microclimate provide testable explanations for the declining relative fungal signal, but neither moisture and aeration nor microbial immigration was measured, and no fallen-culm comparison was included. These factors therefore remain hypotheses rather than explanations supported by the present data. Because fungal-read proportion is a compositional measure, its decline does not establish a decrease in absolute fungal biomass (Gloor et al., 2017). No bacterial phylum showed a significant opposing increase after false-discovery-rate correction; the data therefore identify a declining relative fungal signal but not a specific bacterial lineage replacing fungi.

4.3 Auxiliary redox coding potential declines across decay classes, with divergent taxonomic and AA-family trends

At the community-wide TPM scale based on the unified nonredundant gene catalog, AA-class TPM, the proportion of total CAZy TPM assigned to the AA class, and the TPM of genes assigned to auxiliary redox function all declined across D1–D5., and the direction was preserved under a stricter CAZy annotation threshold. Thus, the data do not support a monotonic increase in auxiliary redox coding potential across the standing dead culm decay classes examined here. The increase in dry-mass lignin concentration and the decline in AA coding potential describe different quantities and should not be treated as opposing measures of the same process. Lignin may become relatively concentrated as other substrate components are lost, whereas AA TPM describes the relative representation of annotated genes in the metagenome. The AA class encompasses functionally heterogeneous redox-enzyme families, including lignin-associated oxidoreductases and lytic polysaccharide monooxygenases acting on polysaccharides; it is therefore not a category of lignin-specific enzymes (Levasseur et al., 2013; Lombard et al., 2014).

The observed decline therefore reflects a change in the AA gene repertoire rather than a lignin-specific functional response. The parallel decline in fungal-assigned AA TPM suggests that changes in the detectable fungal contribution may partly underlie the overall AA trend. However, the present design cannot determine whether this pattern reflects substrate filtering, culm microclimate, microbial immigration, or other differences associated with decay class, so that the predominantly fungal redox repertoire declines rather than increases; this is consistent with the concurrent decreases in the relative fungal signal and in fungal-derived AA discussed below, but remains a hypothesis to be tested against culm moisture, aeration, and absolute fungal quantification.

The inferred direction of AA change is sensitive to how abundance is computed and normalized: uncorrected MAG-weighted values and assembly gene counts indicate an increase in AA, whereas ORF-number normalization and community-wide TPM indicate a decrease. Because far fewer representative MAGs were recovered from D1 and D2 than from other classes, MAG-level functional estimates are more susceptible to differences in assembly and binning efficiency; Community-wide TPM was prioritized because it normalizes for gene length and library size and is not restricted to recovered MAGs. Nevertheless, it remains a relative measure and depends on gene-catalog recovery, sequence mappability, and coverage-dependent gene detection. ORF-normalized, MAG-abundance-normalized, and community-wide TPM analyses showed the same directional decline. Because these analyses share samples and upstream data, their agreement constitutes a sensitivity check rather than independent validation. Residual

differences in metagenome coverage may therefore continue to affect gene-family detection and abundance estimates despite normalization (Aldeguer-Riquelme et al., 2025).

Among AA genes with concordant domain-level assignments, fungal-assigned AA TPM decreased across D1–D5, whereas bacterial-assigned AA TPM increased. The community-wide AA decline therefore comprised divergent trends in the taxonomically assignable fraction rather than a uniform decline across fungal- and bacterial-assigned genes. Previous work combining metagenomics, metatranscriptomics, and nutrient-flux measurements demonstrated complementary fungal and bacterial roles in deadwood decomposition (Tláskal et al., 2021). In contrast, the present DNA-based assignments identify opposing trends in coding potential but do not establish functional complementarity or replacement. The increase in bacterial-assigned AA TPM cannot be interpreted as replacement of fungal ligninolysis because the detected AA families differ in substrate range and catalytic role. Because fungal reads and fungal-derived AA genes derive from the same metagenomic data and share the same detection and annotation constraints, they are not independent evidence; These correlated signals support a change in the taxonomically assignable AA gene pool but do not demonstrate bacterial replacement of fungal oxidative functions.

AA-family trends were heterogeneous: most families with statistically supported trends decreased across D1–D5, whereas AA2, AA15, and AA18 increased. The decline in total AA TPM therefore cannot be generalized to every AA family or catalytic role. Resolving the taxa carrying AA2, AA15, and AA18 and determining whether their increase reflects taxonomic turnover or substrate filtering will require improved genome linkage and taxonomic assignment, together with expression- or enzyme-level measurements.

4.4 Candidate bacterial MAGs provide genomic contexts for bacterial CAZy coding potential

The MAG analysis linked a subset of CAZy genes to recoverable bacterial genomic contexts. Several Granulicella MAGs meeting the D3–D5 descriptive preference criteria carried CAZy families assigned to functional categories related to hemicellulose/xylan, pectin, and oligosaccharides, whereas selected Rhizomicrobium and Rhodopila MAGs carried multiple AA families mapped to auxiliary redox function. The descriptive decay-class abundance profiles of these candidate MAGs are broadly consistent with previous evidence that deadwood-associated bacterial communities vary across decomposition stages and with wood chemistry (Tláskal et al., 2017). However, these observations identify only candidate bacterial genomic contexts for subsequent validation and do not quantify their contribution to the community-wide CAZy trend.

Decay-class preference was defined descriptively from group means and fold-change thresholds without replicate-based differential-abundance testing. Accordingly, the selected MAGs are described as candidate bacterial functional carriers with CAZy coding potential associated with plant-polysaccharide utilization, rather than as significantly enriched taxa or experimentally validated key degraders. Uneven MAG recovery and mapped-read representation further constrain comparisons involving D1 and D2. The selected MAGs should therefore be regarded as candidate functional carriers rather than significantly enriched taxa or key degraders, and the CAZy families detected in them represent coding potential only—they do not demonstrate that the genes are expressed or actually involved in culm degradation, still less that bacteria take over fungal functions.

4.5 Ecological interpretation and study boundaries

The MAG analysis linked a subset of CAZy genes to recoverable bacterial genomic contexts. Several Granulicella MAGs meeting the D3–D5 descriptive preference criteria carried CAZy families assigned to functional categories related to hemicellulose/xylan, pectin, and oligosaccharides, whereas selected Rhizomicrobium and Rhodopila MAGs carried multiple AA families mapped to auxiliary redox function. The descriptive decay-class abundance profiles of these candidate MAGs are broadly consistent with previous evidence that deadwood-associated bacterial communities vary across decomposition stages and with wood chemistry (Tláskal et al., 2017). However, these observations identify only candidate bacterial genomic contexts for subsequent validation and do not quantify their contribution to the community-wide CAZy trend.

The principal constraints of this study were its single-site, cross-sectional design, three composite biological replicates per decay class, and absence of a standing-versus-fallen comparison. Because each replicate pooled material from three culms, the composite sample—not the individual culm—was the analytical unit, and among-culm variation within each decay class could not be estimated. The results therefore establish associations among decay class, substrate chemistry, community composition, and coding potential but do not resolve temporal succession, causal relationships, geographic generalizability, or decomposition fluxes. Moreover, the DNA-based functional analysis describes genomic coding potential rather than gene expression, enzyme activity, or realized metabolic processes. A decisive follow-up would combine longitudinal sampling of marked culm cohorts with paired standing and fallen culms, measurements of culm moisture and mass loss or respiration, absolute fungal and bacterial quantification, metatranscriptomics, and enzyme assays. Such a design would test whether the upright position alters the microbial decomposition trajectory and connect CAZy coding potential to functional activity and carbon flux.

References

Aldeguer-Riquelme, B. et al. Differences in metagenome coverage may confound abundance-based and diversity conclusions and how to deal with them. ISME Communications 5, ycaf140 (2025).

Baldrian, P. Forest microbiome: diversity, complexity and dynamics. FEMS Microbiology Reviews 41, 109–130 (2017).

Bowers, R. M. et al. Minimum information about a single amplified genome (MISAG) and a metagenome-assembled genome (MIMAG) of bacteria and archaea. Nature Biotechnology 35, 725–731 (2017).

Chen, B. et al. Fungal community assembly in standing deadwood: stochastic vs. deterministic processes across decay stages. Environmental Microbiology Reports 17, e70208 (2025).

Cornwell, W. K. et al. Plant traits and wood fates across the globe: rotted, burned, or consumed? Global Change Biology 15, 2431–2449 (2009).

Dong, W. et al. Impacts of litter composition on the structure and functional pathways of soil microbial community during Phyllostachys edulis expansion. Agronomy 12, 220 (2022).

Gloor, G. B. et al. Microbiome datasets are compositional: and this is not optional. Frontiers in Microbiology 8, 2224 (2017).

Harmon, M. E. et al. Ecology of coarse woody debris in temperate ecosystems. Advances in Ecological Research 15, 133–302 (1986).

Hoppe, B. et al. Linking molecular deadwood-inhabiting fungal diversity and community dynamics to ecosystem functions and processes in Central European forests. Fungal Diversity 77, 367–379 (2016).

Huang, X. et al. Effects of on- and off-year management practices on the soil organic C fractions and microbial community in a Moso bamboo (Phyllostachys edulis) forest in subtropical China. Frontiers in Plant Science 13, 1020344 (2022).

Levasseur, A. et al. Expansion of the enzymatic repertoire of the CAZy database to integrate auxiliary redox enzymes. Biotechnology for Biofuels 6, 41 (2013).

Lombard, V. et al. The carbohydrate-active enzymes database (CAZy) in 2013. Nucleic Acids Research 42, D490–D495 (2014).

Mäkipää, R. et al. Interactions between soil- and dead wood-inhabiting fungal communities during the decay of Norway spruce logs. The ISME Journal 11, 1964–1974 (2017).

Perreault, L. et al. Linking wood-decay fungal communities to decay rates: using a long-term experimental manipulation of deadwood and canopy gaps. Fungal Ecology 62, 101220 (2023).

765 Purahong, W. et al. Molecular evidence strongly supports deadwood-inhabiting fungi exhibiting
766 unexpected tree species preferences in temperate forests. The ISME Journal 12, 289–295 (2018).
767 Shi, L. et al. Mixed leaf litter decomposition and N, P release with a focus on Phyllostachys
768 edulis (Carrière) J. Houz. forest in subtropical southeastern China. Acta Societatis Botanicorum
769 Poloniae 84, 207–214 (2015).
770 Shorohova, E. et al. Coarse woody debris density and carbon concentration by decay classes in
771 mixed montane wet tropical forests. Biotropica 54, 635–644 (2022).
772 Tláskal, V. et al. Bacteria associated with decomposing dead wood in a natural temperate forest.
773 FEMS Microbiology Ecology 93, fix157 (2017).
774 Tláskal, V. et al. Complementary roles of wood-inhabiting fungi and bacteria facilitate deadwood
775 decomposition. mSystems 6, e01078-20 (2021).
776 Tsuyama, T. et al. Quantitative morphological transformation of vascular bundles in the culm of
777 moso bamboo (Phyllostachys pubescens). PLOS ONE 18, e0290732 (2023).
778 van der Wal, A. et al. Neglected role of fungal community composition in explaining variation in
779 wood decay rates. Ecology 96, 124–133 (2015).
780 Weedon, J. T. et al. Global meta-analysis of wood decomposition rates: a role for trait variation
781 among tree species? Ecology Letters 12, 45–56 (2009).
782 Yin, Y. et al. dbCAN: a web resource for automated carbohydrate-active enzyme annotation.
783 Nucleic Acids Research 40, W445–W451 (2012).
784 Zhang, H. et al. dbCAN2: a meta server for automated carbohydrate-active enzyme annotation.
785 Nucleic Acids Research 46, W95–W101 (2018).
786 Zheng, J. et al. dbCAN3: automated carbohydrate-active enzyme and substrate annotation.
787 Nucleic Acids Research 51, W115–W121 (2023).

Supplementary Files

This is a list of supplementary files associated with this preprint. Click to download.

- TableS1decaygradientstatistics.xlsx
- TableS1substratechemistrybysample.xlsx
- TableS2alphadiversity.xlsx
- TableS2betadisperpermutest.xlsx
- TableS2dominantphylumtrends.xlsx
- TableS2PERMANOVAadonis2.xlsx
- TableS2phylumrelativeabundance.xlsx
- TableS3117bacterialMAGmastertable.xlsx
- TableS4candidatekeycarriers.xlsx
- TableS6stagepreferencedefinitionaudit.xlsx
- TableS4roleMAGcarriers.xlsx
- TableS6stagepreferentialMAGcandidates.xlsx